Struct Multidisc Optim (2010) 42:325–340
DOI 10.1007/s00158-010-0510-1

RESEARCH PAPER

Optimization of passive vibration isolators mechanical characteristics

Zuzana Dimitrovová · Hélder C. Rodrigues

Received: 11 October 2009 / Revised: 12 March 2010 / Accepted: 26 March 2010 / Published online: 12 May 2010

Abstract The contribution of optimization has been essential to the more recent developments in design of new mechanical structures and materials. The objective of this work is to apply the models of material and structural optimization to the design of passive vibration isolators. A computational tool to identify the optimal viscoelastic characteristics of a nonlinear one-dimensional isolator was developed. The cost functional involves the minimization of a weighted average of the maximum transient and steady state response amplitudes for a set of predefined dynamic loads. The optimal isolator behaviour is obtained by a simulated annealing method. The solutions obtained are analyzed and discussed concerning their dependence on the applied forces and objective function selection. The results obtained can facilitate the design of elastomeric materials with improved behaviour in terms of dynamic stiffness for passive vibration control.

Keywords Vibration · Control · Viscoelastic · Optimization · Simulated annealing

Presented at 8th World Congress on Structural and Multidisciplinary Optimization, 1–5 of June, 2009, Lisbon, Portugal.

Founded by PTDC/EME-PME/67658/2006.

Z. Dimitrovová
UNIC, Department of Civil Engineering, New University of Lisbon, Lisbon, Portugal

H. C. Rodrigues (✉)
IDMEC, Instituto Superior Técnico, UT Lisbon, Lisbon, Portugal
e-mail: hcr@ist.utl.pt

1 Introduction

The latest developments in computational mechanics lead to integrated methodologies that permit not only the structural design and optimization of the mechanical component but also the tailoring of the material properties and consequently the design of new materials. The aim of this contribution is to extend the techniques of structural and material nonlinear optimization and apply them in the design of isolators and materials for passive vibration control. Passive vibration control typically addresses only attenuation of the steady-state regime of the structure dynamic response. However in some industrial applications, namely automotive applications, the transient regime should also be considered. Here this requirement will be addressed defining objective functions that accommodate contributions from both regimes.

In the steady state case and when the isolator is required to operate on a large frequency range, it would be ideal to have a material that softens and has low damping at high frequencies. Unfortunately, it can be proven that within one phase solid materials what is observed is exactly the opposite, in other words real materials strengthen at high frequencies (Pritz 1998). Therefore in this case it is necessary to design new "composite" materials with specific dynamic properties, namely, a material that softens at high frequencies (Prasad and Diaz 2008). To address this problem and following the works of Lakes (2001, 2002), Prasad and Diaz (2008) developed a model, requiring the introduction of components with negative stiffness, to synthesize periodic materials with a frequency softening behaviour. Mechanical components exhibiting negative stiffness are usually realized by means of structures with snap-through instability (Jirásek 1988). Also recent studies on quasi-zero stiffness isolation, i.e. where at the equilibrium force

level there is a plateau in the force-displacement diagram, become the focus of research efforts and industrial interest (Platus 1993; Kovacic et al. 2008).

Here we will address both regimes, transient and steady state thus a different path was taken. A computational tool to determine the macroscopic optimized one-dimensional isolator behaviour was developed. The objective function controls displacement and/or force reaction and has contributions from both regimes; transient and steady state. Material stiffness parameters are assumed as nonlinear functions of displacement. Steady-state solution is obtained by an iterative process based on the shooting method and imposing the conditions of periodicity on known value of the period (Jirásek 1988). The material parameters characterizing the nonlinear behaviour are then optimized by a generic probabilistic metaheuristic algorithm, simulated annealing.

The paper is organized as follows. In Section 2 the problem statement is given. Then the computational tool developed is described in details, regarding the possibilities which are currently implemented in the code, namely load cases, objective function selection and material models. Section 3 describes the techniques used for numerical implementation. Section 4 presents and discusses the results obtained. Paper conclusions are presented in Section 5.

The results attained, although still related only to one-dimensional behaviour, are mechanically significant and can help the design of elastomeric cellular/composite materials with improved behaviour for passive vibration control. Future research will be directed to optimization of multidirectional properties, which will be used as target behaviour for design of cellular and/or composite viscoelastic materials.

2 Computational tool

2.1 Problem statement

For analysis and design purpose we assumed that a mass of a given value, M, is connected through a passive isolator $S(u, \dot{u})$, function of displacement u and velocity $\dot{u}$, to a fixed support. The mass is excited by a time dependent set of forces, $P(t)$. The objective is to determine the isolator characteristics which will provide an optimal dynamic performance of the system. The model is schematically represented in Fig. 1.

Following engineering practical requirements, the reaction exerted by the support, $R(t)$, and the displacement exhibited by the mass, $u(t)$, are the decisive criteria for optimization (see e.g. Balandin et al. 2001). In terms of time

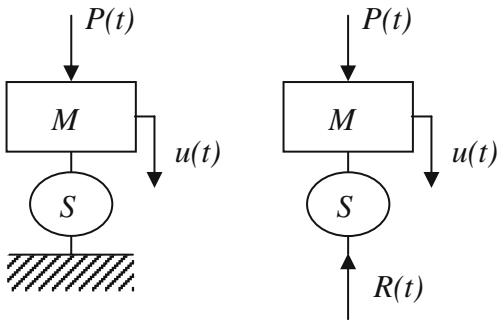

Fig. 1 Isolation system problem definition

dependence it is possible to identify two regimes; transient and the steady-state respectively. Based on this partition the optimization goal is to minimize $u(t)$ and/or $R(t)$ "amplitudes" in both regimes. Here the term "amplitude" identifies the maximum response (displacement or force) difference in each regime.

The computational tool developed to identify the optimal one-dimensional isolator mechanical characteristics, can be specialized depending on the load cases, the particular objective function and the material model assumed. All possibilities currently available will be described in the following sections, although the results presented will correspond only to some particular scenarios. It is, however, important to list all the options currently available. Their description will be given in the following order: (1) load cases; (2) objective function; (3) material models and admissible isolator behaviour.

2.2 Load cases

Let us define the applied forces and load cases which are possible to introduce in the code. They were selected according to practical situations as: (i) single step load, (ii) set of step loads, (iii) single step load with harmonic component, (iv) set of step loads with harmonic components (see e.g. Zavala et al. 2000). Load cases (i) and (iii) (single load cases) are depicted in Fig. 2.

Here P_0 stands for the value of the applied step load, the harmonic component can be expressed by $P_1 \sin(\omega t + \phi)$, where P_1 is the amplitude, ω the circular frequency and ϕ the phase angle.

Load cases (ii) and (iv) correspond to a set of "q" discrete loads, where the respective weights λ_i, satisfying $\sum_{i=1}^{q} \lambda_i = 1$, must be defined according to given criteria such as importance of the particular load or probability of occurrence.

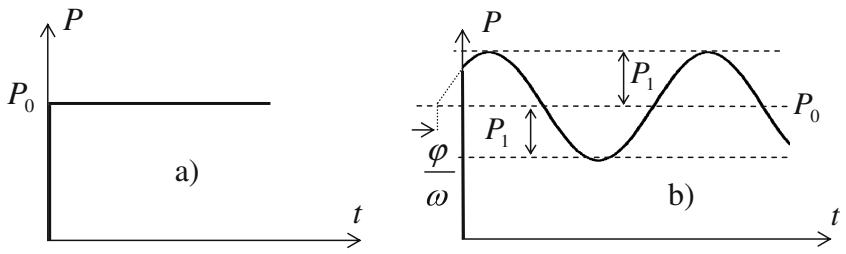

Fig. 2 Schematic representation of load cases: **a** load case (i); **b** load case (iii)

2.3 Objective function

The objective function considered for the load cases (i) and (iii) is given as:

$$O(S(u,\dot{u})) = \gamma_{tr} \underset{t\in\langle 0;t_r\rangle}{A_{tr}} + \gamma_{st} \underset{t\in\langle t_r;tf\rangle}{A_{st}}, \tag{1}$$

where $O(S(u,\dot{u}))$ is the objective function value related to some admissible isolator behaviour $S(u,\dot{u})$, t_r is the time separating transient and steady-state regimes and t_f identifies the final time. In (1) A_{tr} and A_{st} are the transient and steady-state regime contributions to the objective function weighted respectively by the coefficients γ_{tr} and γ_{st}, satisfying $\gamma_{tr} + \gamma_{st} = 1$.

In more detail A_{tr} and A_{st} are given by:

$$\begin{aligned} A_{tr} &= \frac{\alpha_{tr}}{\|R\|}\left(\max_{t\in\langle 0;\,t_r\rangle} R(t) - \min_{t\in\langle 0;\,t_r\rangle} R(t)\right) \\ &\quad + \frac{1-\alpha_{tr}}{\|u\|}\left(\max_{t\in\langle 0;\,t_r\rangle} u(t) - \min_{t\in\langle 0;\,t_r\rangle} u(t)\right), \\ A_{st} &= \frac{\alpha_{st}}{\|R\|}\left(\max_{t\in\langle t_r;\,t_f\rangle} R(t) - \min_{t\in\langle t_r;\,t_f\rangle} R(t)\right) \\ &\quad + \frac{1-\alpha_{st}}{\|u\|}\left(\max_{t\in\langle t_r;\,t_f\rangle} u(t) - \min_{t\in\langle t_r;\,t_f\rangle} u(t)\right). \end{aligned} \tag{2}$$

The weights α_{tr} and α_{st} express the relative importance of the reaction versus displacement in each regime and $||R||$, $||u||$ are convenient norms related to the particular application.

All parameters and weights γ_{tr}, γ_{st}, α_{tr}, α_{st}, $||R||$, $||u||$ are user input values and permit the objective function specialization for a large set of practical situations.

It is interesting to analyse some special cases. For step load (1), $\gamma_{st} = 0$ because there is no steady-state response, while for a step load with harmonic component (3) both weights γ_{tr} and γ_{st} can be assumed non-zero. If only the reaction contribution in the steady-state regime is considered, i.e. if $\gamma_{tr} = 0$ and $\alpha_{st} = 1$, the objective function value is proportional to the transmissibility T. In fact if one defines $||R|| = 2P_0$ then:

$$O(S(u,\dot{u})) = \frac{1}{2P_0}\left(\max_{t\in\langle t_r;t_f\rangle} R(t) - \min_{t\in\langle t_r;t_f\rangle} R(t)\right) = T. \tag{3}$$

For the load cases (ii) and (iv) it is assumed that the objective function is given by:

$$O(S) = \sum_{i=1}^{q} \lambda_i O_i(S), \tag{4}$$

where, as already mentioned, the weights λ_i, satisfying, $\sum_{i=1}^{q} \lambda_i = 1$, must be set according to the importance of the particular load or probability of occurrence.

Once defined the objective function, the optimization procedure searches for the optimal isolator behaviour $S^*\left(u,\dot{u}\right)$, which solves the optimization problem

$$Ot(S^*) = \min_{S\,\in\,\Xi} O(S), \tag{5}$$

where Ξ defines the set of admissible isolator behaviours.

2.4 Material models and admissible isolator behaviour

Material models currently implemented in the code are Voigt, Maxwell and Standard Material models (Jones 2001). In each of these cases the spring part is assumed nonlinear elastic. All dampers are assumed linear viscous characterized by the damping coefficient C. From these assumptions the isolator can be schematically identified with the systems shown in Fig. 3, where $F(u(t))$ stands for the elastic force of the nonlinear spring, C is the damping constant of the linear damper and the "dot" identifies the time derivative.

Here we will restrict the presentation to the Voigt model, the one used in the examples presented. For this case the system equation of motion is given as (Meirovitch 1975):

$$M\ddot{u}(t) + C\dot{u}(t) + F(u(t)) = P(t) + Mg, \tag{6}$$

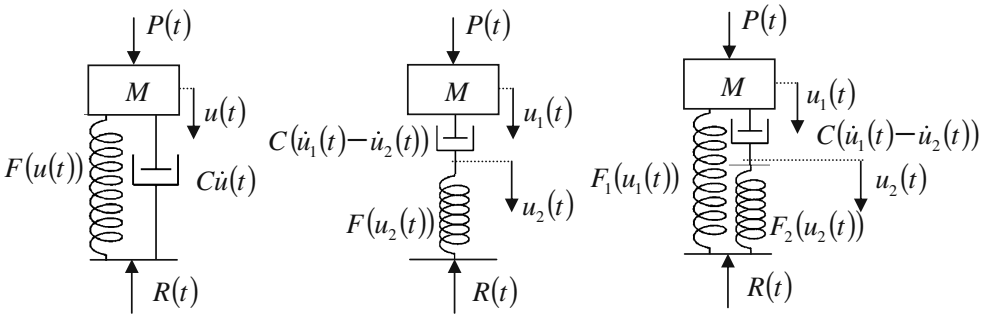

Fig. 3 Schematic representation of the isolator in form of Voigt, Maxwell and standard material model

where g is the acceleration of gravity. Setting the "zero" displacement at the static equilibrium position, one gets

$$M\ddot{u}\,(t) + C\,\dot{u}\,(t) + F\,(u\,(t)) = P\,(t)\,, \tag{7}$$

where for simplicity the displacement designation was maintained.

The support reaction is given by:

$$R\,(t) = C\,\dot{u}\,(t) + F\,(u\,(t))\,. \tag{8}$$

The admissible isolator behaviour, i.e. the design domain "Ξ" definition, involves setting the range of possible values of the damping coefficient C and defining the allowable nonlinear behaviour for the respective material model spring, i.e. the domain of allowable load-displacement curves.

Due to the assumed linear viscous behaviour, C specification requires only numerical values definition; therefore it will be done in the results section. On the other hand the admissible load-displacement curves must satisfy not only physico-mathematical requirements but also functional ones. Practical applications imply that the spring rigidity is not fully arbitrary and that fixed and variable parts of the load-displacement curve must be identified. Here we will assume that the spring load displacement diagram has initial and final linear parts. The initial part is specified by a fixed stiffness value K_{ini} that should be set based on the allowed initial static displacement of the mass. The final part is characterized by a value K_{fin}, which must be greater or equal than given lower bound value $\bar{K}_{fin}$. This portion will actuate when the maximum displacement u_{ma} value is surpassed so the $\bar{K}_{fin}$ value should be set to control the maximum displacement violation. Additionally it is imposed that at the maximum displacement u_{ma} value, the force cannot exceed an admissible value F_{ma}. To illustrate this, three admissible nonlinear spring designs are shown in Fig. 4, where the variable (dashed, dash-dotted) part of the load-displacement curve is the focus of optimization. The dotted line identifies the "reference" load-displacement curve, piecewise linear defined by slope values K_{ini}, K_{ref} and $K_{fin} = \bar{K}_{fin}$, that will be used further on for comparison analyses with the obtained final ("optimal") solutions.

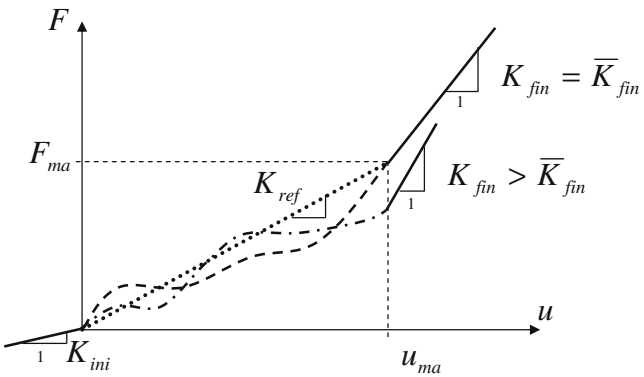

Fig. 4 Load-displacement curve for three possible non-linear spring designs. Fixed parts (*solid*) and variable/designable parts (*dashed*, *dash-dotted*, *dotted*)

Besides these functional constraints the load-displacement curve must satisfy the following mathematical requirements in the interval $\langle 0, u_{ma}\rangle$:

1. It must be continuous;
2. It must be monotonically increasing, i.e. stiffness must be non-negative at any displacement value, to avoid dynamic instability;
3. Spring behaviour is perfectly hyperelastic, i.e. loading and unloading paths match exactly.

3 Numerical implementation

The computational tool is developed in Matlab environment (MATLAB 2007). This section describes the actual numerical implementation of the concepts specified in Section 2. It covers: (1) the load-displacement curve definition; (2) the solution of the governing equations; (3) the extraction of the objective function value; (4) the optimization procedure

and (5) assessment of the efficiency and the sensitivity of the "optimal" design.

First of all it is necessary to introduce the interpolation of the load-displacement curve and assure its admissibility. The approach taken is the following:

1. Select a set of fixed points u_i, $i = 1, \ldots, n$ from the given open interval $(0, u_{ma})$, assign $u_0 = 0$ and $u_{n+1} = u_{ma}$ (uniform distribution can be used $\Delta u = u_{i+1} - u_i$);
2. Randomly select force values F_i, $i = 1, \ldots, n+1$ from the given interval $]0, F_{ma}]$, order them in an increasing way and attribute them to the points u_i ($F_0 = 0$);
3. Define a spline interpolation within each interval $\langle u_i, u_{i+1} \rangle$, $i = 0, \ldots, n$.

As far as possible spline approximations, linear and cubic Hermite approximations were tested for suitability. Linear spline approximation preserves continuity and easily guarantees monotonic behaviour. However it does not preserve stiffness continuity at the interpolation points u_i. On the other hand cubic Hermite approximation preserves continuity and stiffness continuity at u_i, but monotonicity is not so easily enforced. To assure monotonicity in this case we adopted the methodology described by Fritsch and Carlson (1980).

The two possible spline approximations described were tested for accuracy and computational time. No significant differences were found. Existence and continuity of the first derivative was not a load-displacement curve requirement. Nevertheless, it is necessary to point out, that in cases where periodic solution of the governing equations is established by the shooting method (described in Appendix A), it is necessary to use the cubic Hermite approximation.

Solution of the governing equations is obtained using the ODE45 Matlab solver. Whenever necessary, periodic solution corresponding to the steady-state regime is approached by the shooting method (for more details see Appendix A). After that the value of the objective function can be easily extracted.

As an alternative to the shooting method it is also possible to implement the so called "method of a long simulation", i.e. the dynamic response is recorded for a sufficiently long time interval in order to ensure that the transient (the natural vibration) part of the response is completely damped out. This procedure has obviously several disadvantages: (1) it is difficult to a priori estimate the time interval needed for the evaluation because it is design dependent (see (1) where t_r and t_f were introduced); (2) the method is unusable in undamped systems; (3) it may be time consuming and (4) it may increase numerical error due to the long time interval required.

Simulated Annealing (SA) was chosen as the optimization tool (Kirkpatrick et al. 1983). The general steps can be briefly described as follows. Let us consider iteration "k" with the respective load-displacement curve $F^{(k)}$ and objective function value $O^{(k)}$. Then for the next iteration "$k+1$" a new load-displacement curve in the "neighbourhood" of the old one is created and the respective objective function value $O^{(k+1)}$ computed. If $O^{(k+1)} < O^{(k)}$ then the new load-displacement curve $F^{(k+1)}$ is unconditionally accepted. Otherwise, if $O^{(k+1)} \geq O^{(k)}$ then it is conditionally accepted, based on a probability randomly selected from the interval (0, 1) and compared with the value calculated from $\exp((O^{(k)} - O^{(k+1)})/T_j)$, where T_j is the current cooling temperature. This acceptance of "worse designs" facilitates the search through the entire design domain and is crucial to avoid local minimums. It is called the Metropolis criterion. As the cooling proceeds, the cooling temperature lowers and consequently the conditional acceptance probability decreases.

Like any probabilistic metaheuristic algorithm, Simulated Annealing (SA) has some parameters which must be carefully chosen as they can alter the final result and/or make the calculation inefficient. They are:

1. The initial temperature;
2. The number of iterations within each temperature;
3. The cooling schedule;
4. The stopping criteria;
5. The neighbourhood definition.

Neighbourhood definition is a crucial aspect in a SA algorithm. If too wide the optimization procedure might jump from one region to another without the possibility of finding an optimum design. When too narrow, then the search is limited to a small region around the actual design and the program may converge to a local optimum. In our application the neighbourhood of the current load-displacement curve is formed by all load-displacement curves whose design forces lay within a specified interval. This interval is defined based on two user defined parameters, the perturbation value $0 < p < 1$ and the number of design force values allowed to vary $m (\leq n)$. Recall that "n" designates the total number of design forces. For a chosen perturbation p the interval around design force F_i is defined as $\langle F_i - pF_{ma}/2;\ F_i + pF_{ma}/2 \rangle$, with obvious lower and upper constraints at "0" and F_{ma}, respectively.

This process is numerically implemented in the following way:

1. At "m" random positions a random force value is selected from the interval given above;
2. After the new force values are obtained they are ordered in an increasing way, to satisfy the monotonicity requirement.

To analyze the final ("optimal") solution efficiency, a comparison with the value obtained for the "reference design" (defined in Section 2.4 and Fig. 4 dotted line) is performed. Efficiency E is expressed as:

$$E = \frac{O_{ref} - O_{fin}}{O_{ref}}, \tag{9}$$

where O_{fin} is the final design objective function value and O_{ref} is the value obtained for the reference design. It is worthwhile to point out that it is impossible to apply shooting method on the reference design, therefore, steady-state solution can only be obtained by the "method of long simulation".

Additionally to assess the final ("optimal") design reliability a design "sensitivity" analysis is performed as follows. A perturbation of the final design is imposed by a 1% design point perturbation from its optimal value (same definition as for the neighbourhood). One thousand perturbations with randomly selected design points are evaluated and histograms of the disturbances in the objective function value are analyzed. The disturbance is defined as:

$$d = \frac{O_{pert} - O_{fin}}{O_{fin}}, \tag{10}$$

where O_{pert} stands for the objective function value of the perturbed design.

Due to the complexity of the numerical tool developed, it is impossible to draw clear conclusions from case studies that mix all the options available. Therefore, this paper is restricted only to Voigt material model. Moreover, optimization is restricted only to the total dynamic reaction, thus $\alpha_{tr} = \alpha_{st} = 1$ and then dimensionless $||R|| = 1$ can be taken (see (2)). Further analyses involving other case studies will be presented in subsequent works.

4 Results

In this section several case studies are analysed. They are grouped in four subsections according to the load cases introduced in Section 2.2 as: (i) single step load, (ii) set of step loads, (iii) single step load with harmonic component, and (iv) set of step loads with harmonic components (compare with Fig. 2). First of all it is essential to introduce realistic numerical input data namely for the definition of the (1) load cases; (2) admissible load-deflection curves; (3) values of damping coefficient and (4) parameters related to the simulated annealing procedure.

According to data available for automotive applications, step load value P_0 can be assumed within the interval $\langle 500; 1500 \rangle$N, amplitude of the harmonic component P_1 within the interval $\langle 100; 500 \rangle$N and the excitation frequencies f are within $\langle 25; 250 \rangle$Hz, with $\omega = 2\pi f$.

Values defining the load-displacement curve can be extracted from the same applications as: $u_{ma} = 10$ mm, $F_{ma} = 1{,}500$ N, $K_{ini} = 100$ kN/m and $\bar{K}_{fin} = 1MN/m$, thus giving $K_{ref} = 150$ kN/m (see Fig. 4).

To complete the design space identification it is necessary to specify the number of the design values, we chose $n = 30$. It is moreover assumed that the mass of the object to be isolated is $M = 50$ kg and the damping coefficient C is taken from the interval $\langle 100; 400 \rangle$N.s/m. We recall that C value is not object of optimization, therefore the selected value is kept constant throughout the optimization. Also the same C value is used in the reference design to obtain the respective O_{ref}.

Parameters introduced in the simulated annealing procedure are the following: the initial temperature is chosen as 10% of the initial value of the cost functional. The number of iterations at each temperature level is chosen as 500. 50% decrease of the temperature is used for the cooling schedule. Ten temperature levels are implemented.

Such a low number of temperature levels is related to the fact, that from the sensitivity analysis of the results obtained, the Metropolis criterion can "harm" in some cases the final value of the objective function O_{fin}. Therefore the following strategy is adopted. First optimization run, i.e. the first 10 temperature levels are done with a wider neighbourhood definition (e.g. $m = 10$, $p = 0.2$) and initial load-displacement curve randomly generated. After that the improvement in objective function is analysed. If the improvement is not significant, then the optimization is run again from the final design obtained and with all parameters unchanged. If it is significant, then the final design is refined on a tighter neighbourhood ($m = 1$, $p = 0.1$ or less) with Metropolis criterion deactivated.

As usual, the algorithm can stop before completing the cooling schedule, whenever the number of consecutive failures reaches the user-input number.

4.1 Load case (i)—single step load

This load case corresponds to application of one step force with total value P_0. Within the admissible interval two particular values were selected: $P_0 = 1{,}000$ N and $P_0 = 1{,}200$ N. Regarding damping and to analyse its effect, three values were chosen namely $C = 400$, 200 and 100 N.s/m, yielding the total of 6 tested cases. Linear spline interpolation was implemented in the load-displacement admissible curves, because in this case there is no steady-state regime and therefore the shooting method, requiring the derivative continuity, is not implemented.

Before the results discussion, one should analyze this case in order to "guess" what to expect from the optimization. Let us consider a mass M supported by a linear spring of rigidity K and subjected to a step load. This case has analytical solution and the maximum reaction doubles the applied force at the same time as the maximum displacement is reached. This is simply justified by energy comparison:

$$0 = \frac{1}{2} K u_{\max}^2 - P_0 u_{\max} \quad \Rightarrow \quad u_{\max} = \frac{2P_0}{K}, \; R_{\max} = 2P_0, \tag{11}$$

where $u_{\max}$ and $R_{\max}$ stand for the maximum displacement and the maximum reaction. If damping is included, then the reaction peak value decreases with increasing damping, and it is reached sooner than the maximum displacement. Such case has also analytical solution, (see e.g. Meirovitch 1975). The lowest reaction peak is attained for the highest damping. This case will be in the supercritical damping regime, when $C \geq C_{cr} = 2M\omega_0 = 2\sqrt{KM}$. In our case, the viscous damping coefficient C is a fixed parameter, thus the rigidity must be decreased in order to achieve supercritical damping conditions. Therefore from optimization one might expect a plateau, in the load-displacement curve, at the value of the applied force with displacements covering the full plateau interval $u(t) \in (0, u_{ma})$ but not surpassing its limits. On the other hand the perfect plateau is not possible because the load-displacement curve in the design region must have some rigidity to keep the displacement below u_{ma}, and thus avoid reaction force peaks due to the higher final rigidity K_{fin}.

Adapting (11) to the nonlinear damped case, the maximum displacement is:

$$u_{\max} = \frac{1}{P_0} \int_0^{u_{\max}} R\,(u)\, du. \tag{12}$$

The integral in (12) corresponds to the integral of the load-displacement curve plus the energy loss due to damping. It is impossible to evaluate it before the analysis, but it allows for estimates. The higher the damping coefficient, the higher the energy loss and thus the load-displacement curve rigidity can be lower. When damping is low, localized high rigidity must be formed around the equilibrium position to increase the energy loss in the region where the velocity is highest.

Table 1 Summary of the optimization results: step force $P_0 = 1{,}000$ N

C (N.s/m)	O_{fin} (N)	O_{ref} (N)	E (%)
400	18.4	2,351	99
200	26.4	2,768	99
100	138.2	3,021	95

Table 2 Summary of the optimization results: step force $P_0 = 1{,}200$ N

C (N.s/m)	O_{fin} (N)	O_{ref} (N)	E (%)
400	22.4	3,258	99
200	37.2	3,716	99
100	187.0	3,960	95

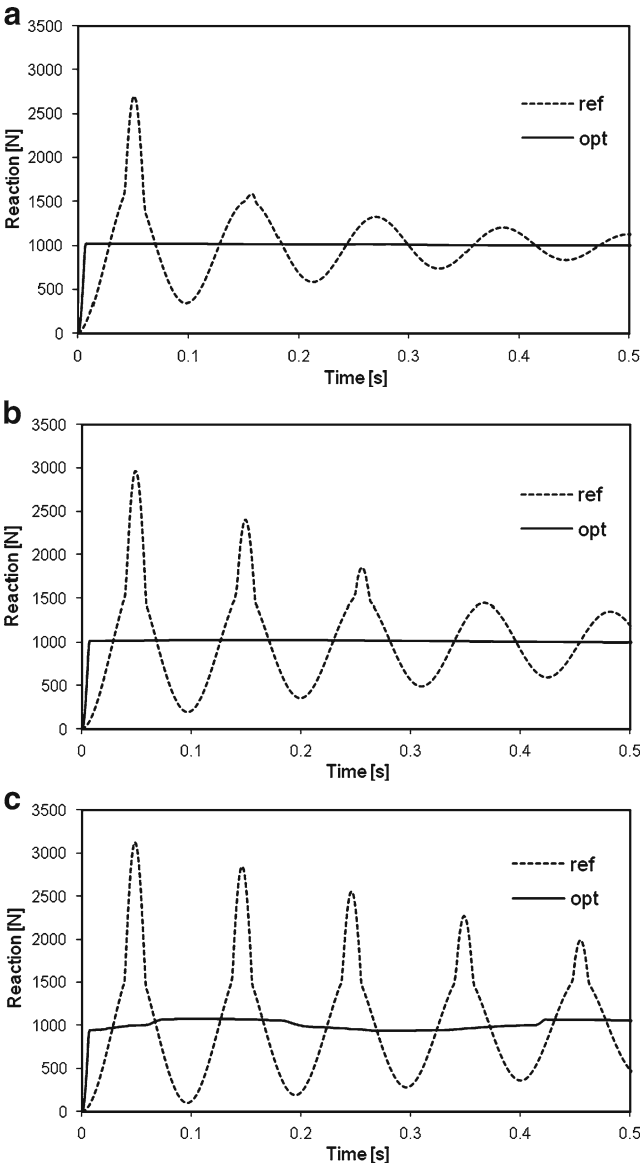

Fig. 5 Total reaction of the reference (*dotted line*) and the optimized designs (*solid line*) for $P_0 = 1{,}000$ N and: **a** $C = 400$ N.s/m, **b** $C = 200$ N.s/m, **c** $C = 100$ N.s/m

These predictions are confirmed by the optimization procedure. Tables 1 and 2 summarize the results obtained for the two step force values, $P_0 = 1{,}000$ N and $P_0 = 1{,}200$ N and the damping coefficient $C = 400$, 200 and 100 N.s/m. Several optimization runs were performed for each of the 6 combinations. All of them gave approximately the same final result. The best objective function value O_{fin} is presented in Tables 1 and 2. This value is compared with the reference case value O_{ref} and the efficiency E is evaluated according to (9).

As expected, the "optimum" objective function value increases with decreasing damping. For the "optimal" design the reaction peak practically disappears, (see Fig. 5).

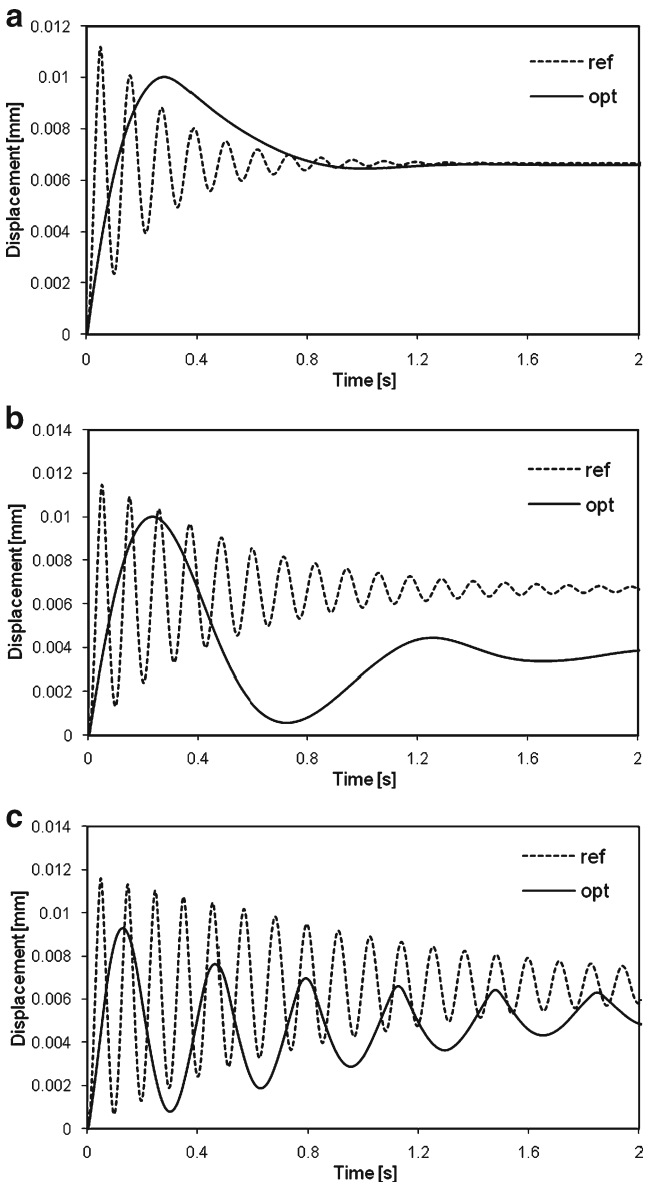

Fig. 6 Displacement of the reference (*dotted line*) and the optimized designs (*solid line*) for $P_0 = 1{,}000$ N and: **a** $C = 400$ N.s/m, **b** $C = 200$ N.s/m, **c** $C = 100$ N.s/m

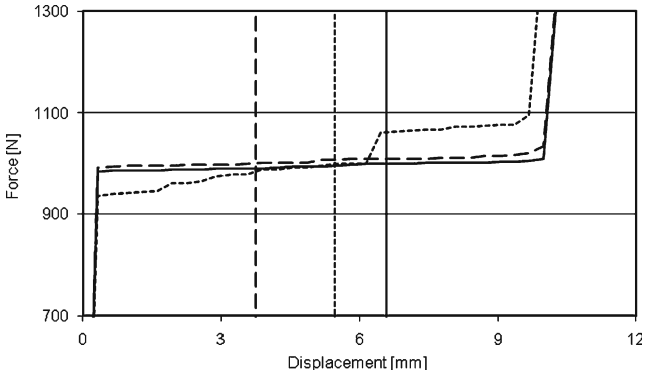

Fig. 7 Final design of the load-displacement curves (detail of the plateau) with the equilibrium displacement designated by the vertical line, step force $P_0 = 1{,}000$ N ($C = 400$ N.s/m *solid line*, $C = 200$ N.s/m *dashed line*, $C = 100$ N.s/m *dotted line*)

The damping influence on the dynamic reaction and on the displacement of the reference and optimized design is easily seen in Figs. 5 and 6, by comparing the respective (a), (b) and (c) figures.

Figures 7 and 8 compare the plateau in optimized designs for the two examined step forces and different C values. The equilibrium displacement is marked by a vertical line. It corresponds to the final displacement value where the vibration is attenuated. At this position static equilibrium must be satisfied therefore the vertical line must cross the load-displacement curve at the applied force level P_0.

As indicated in Section 3 "optimal" design sensitivity analyses were performed. Results of the disturbance defined in (10) are shown in Fig. 9 for the step force $P_0 = 1{,}000$ N and three different values of the damping coefficient C. Disturbance is expressed in % and only values below 150% are shown, (the number of cases with values above this limit is not significant). One thousand tests were run in each case. Graphs in Fig. 9 show a regular pattern with around 50% of the perturbed designs having an objective function increase

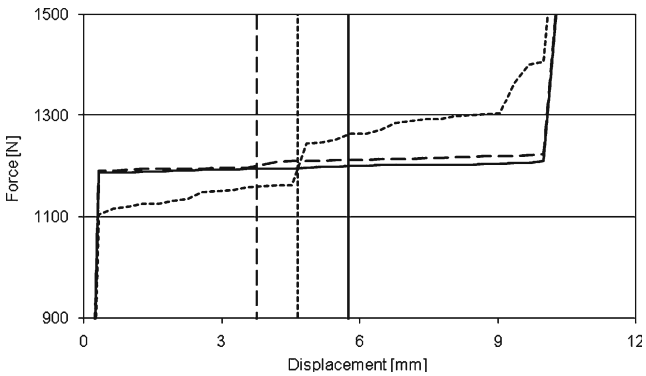

Fig. 8 Final design of the load-displacement curves (detail of the plateau) with the equilibrium displacement designated by the vertical line, step force $P_0 = 1{,}200$ N ($C = 400$ N.s/m *solid line*, $C = 200$ N.s/m *dashed line*, $C = 100$ N.s/m *dotted line*)

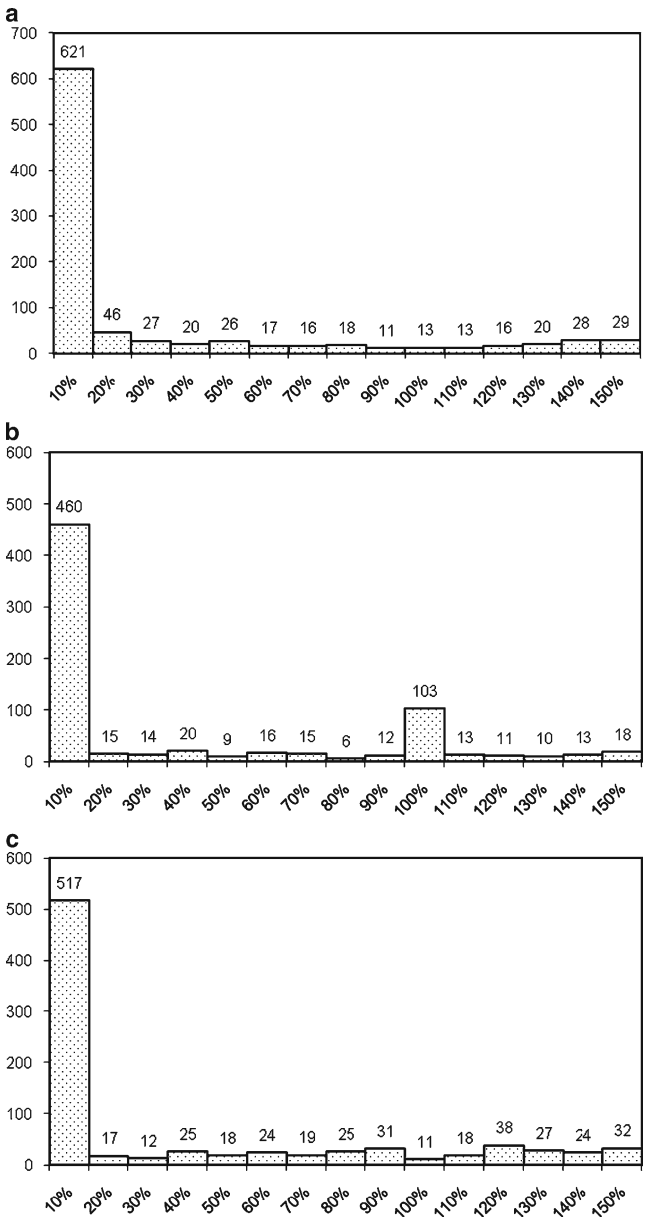

Fig. 9 Histogram of the disturbance value d defined by (10) for $P_0 =$ 1,000 N and: **a** $C = 400$ N.s/m, **b** $C = 200$ N.s/m, **c** $C = 100$ N.s/m

lower than 10%. From this analysis it is visible that the final optimized design is relatively stable, because even 150% increase in the optimized value means still efficiency around of 98%, 98% and 89%, respectively for the three C values.

Table 3 Comparison O_{pl} (objective function value for perfect plateau) O_{fin} (objective function value for "optimal design") for $P_0 = 1{,}000$ N

C (N.s/m)	O_{pl} (N)	O_{fin} (N)
400	31.7	18.4
200	303.0	26.4
100	941.8	138.2

Table 4 Comparison O_{pl} (objective function value for perfect plateau) O_{fin} (objective function value for "optimal design") for $P_0 = 1{,}200$ N

C (N.s/m)	O_{pl} (N)	O_{fin} (N)
400	61.8	22.4
200	477.3	37.2
100	1,119.2	187.0

Histograms of the disturbance for the step force $P_0 =$ 1,200 N have a similar profile.

The next analysis confirms that the perfect plateau is not an optimal design. Tables 3 and 4 compare the objective function final ("optimal") value O_{fin} (from Tables 1 and 2) with the respective value for the "perfect plateau design" O_{pl}.

The difference is caused by reaction peaks that occur in the case of the perfect plateau when the displacement falls beyond the admissible design interval $(0, u_{ma})$ and "activates" the higher rigidity.

4.2 Load case (ii)—set of step loads

This load case corresponds to application of several step loads, weighted by a probability of occurrence λ (compare with (4)). For comparison purposes, two single step loads analysed in the previous section ($P_{0,1} = 1{,}000$ N and $P_{0,2} = 1{,}200$ N) are assumed to occur with the same probability $\lambda_1 = \lambda_2 = 0.5$. Regarding the damping coefficient, as in the previous sections, three values were considered as $C = 400$, 200 and 100 N.s/m.

Results are summarized in Table 5. The total values of the objective function as well as the weighted contributions of each single load are presented. The best value obtained O_{fin} is compared with the reference case (O_{ref}) and efficiency E is calculated according to (9). Significant improvement is verified.

It is useful to evaluate the overall performance of the optimization procedure. For this it is clear that the weighted sum

Table 5 Summary of the optimization results of the load case (ii)

C (N.s/m)		O_{fin} (N)	O_{ref} (N)	E (%)
400	O	220.2	2,804	92
	$\lambda_1 O_1$	73.0	1,175	94
	$\lambda_2 O_2$	147.2	1,629	91
200	O	358.1	3,242	89
	$\lambda_1 O_1$	147.0	1,384	89
	$\lambda_2 O_2$	211.0	1,858	89
100	O	547.8	3,490	84
	$\lambda_1 O_1$	209.1	1,510	86
	$\lambda_2 O_2$	338.7	1,980	83

Table 6 Comparison according to (13)

C (N.s/m)	$O_{fin} = \lambda_1 O_1 + \lambda_2 O_2$ (N)	$\lambda_1 O_{1fin} + \lambda_2 O_{2fin}$ (N)	O_{1fin} (N) $P_{0,1} = 1{,}000$ N	O_{2fin} (N) $P_{0,2} = 1{,}200$ N
400	220.2	20.4	18.4	22.4
200	358.1	31.8	26.4	37.2
100	547.4	162.6	138.2	187.0

of objective function final values, obtained for each load considered individually, is a lower bound to the final objective function obtained for the load case corresponding to the weighted sum of the single loads, O_{fin}. In our case this implies,

$$O_{fin} = \lambda_1 O_1 + \lambda_2 O_2 \geq \lambda_1 O_{1fin} + \lambda_2 O_{2fin}. \tag{13}$$

Values O_{1fin} and O_{2fin} can be obtained from Tables 1 and 2, because they correspond to the load case (i) optimization. The "gap" in inequality (13) gives useful information about optimization procedure global efficiency. The values attained are shown in Table 6.

It is seen that the inequality gap is very large. This means that the plateau formation at the respective equilibrium force levels is not assured. The reason is that the "optimal" design for each load, individually considered, gives a long plateau, practically covering fully the design domain. When there are two different applied forces, this is obviously not reasonable. There is a slightly noticeable plateau at the lower force level $P_{0,1} = 1{,}000$ N, but then the spring needs to accumulate sufficient strain energy to avoid the rigidity increase outside the designable domain. Thus the second plateau is significantly higher than the second applied step force $P_{0,2} = 1{,}200$ N worsening the system performance. For more step loads the situation is generally worse with less efficient final designs. On the other hand this lower effectiveness implies lesser sensitivity. Therefore histograms of the disturbance do not show such large discrepancy as in load case (i).

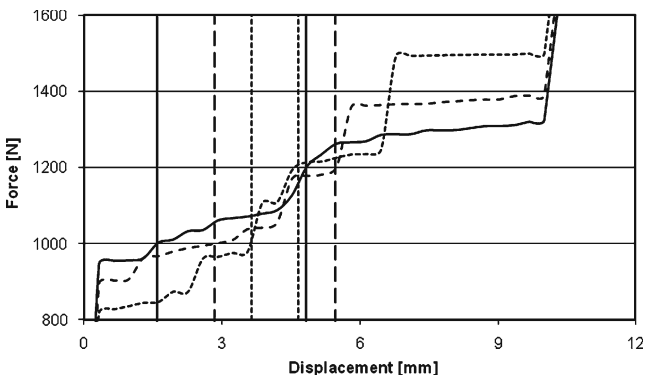

Fig. 10 Final designs of the load-displacement curves with the equilibrium displacement designated by the vertical line for three different damping coefficients $C = 400$, 200, 100 N.s/m represented by *solid*, *dashed* and *dotted line*, respectively

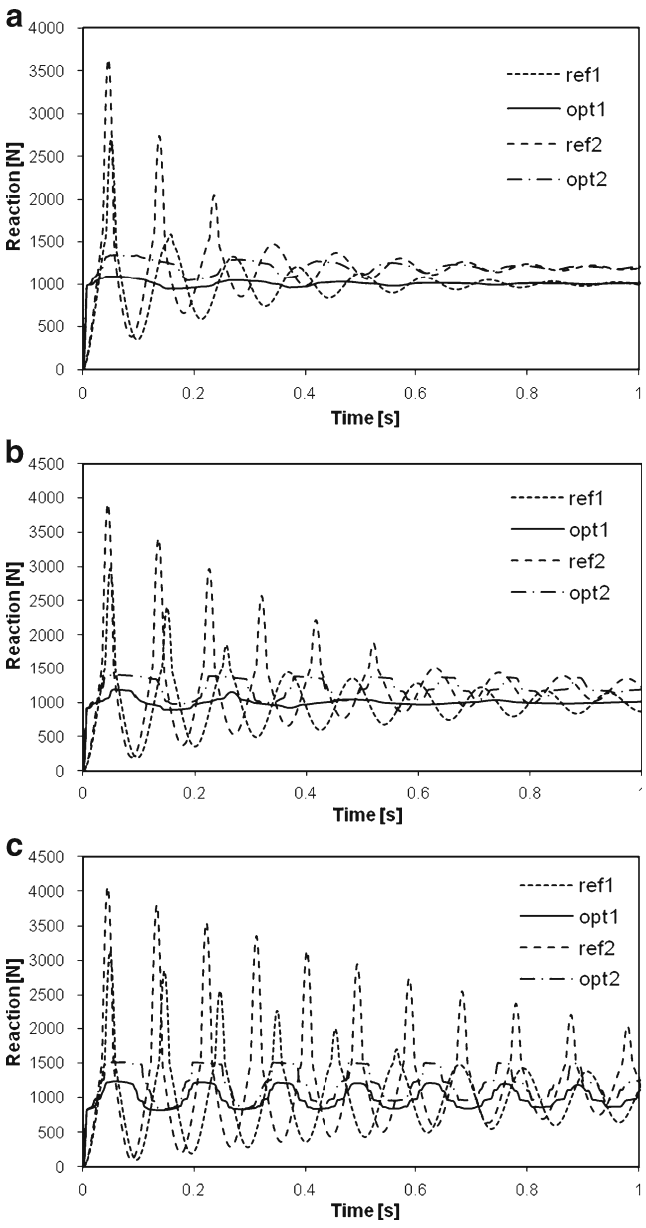

Fig. 11 Total reaction of the reference (*dotted line* for $P_{0,1}$ and *dashed line* for $P_{0,2}$) and the optimized designs (*solid line* for $P_{0,1}$ and *dash-dotted line* for $P_{0,2}$): **a** $C = 400$ N.s/m, **b** $C = 200$ N.s/m, **c** $C = 100$ N.s/m

Optimised load-displacement curves are shown in Fig. 10.

Comparison of the dynamic reaction and of the displacement is shown in Figs. 11 and 12, respectively. Histograms of the disturbance are reported in Fig. 13.

4.3 Load case (iii)—single step load with harmonic component

This load case considers one step force with one harmonic component, thus the loading function can be written as

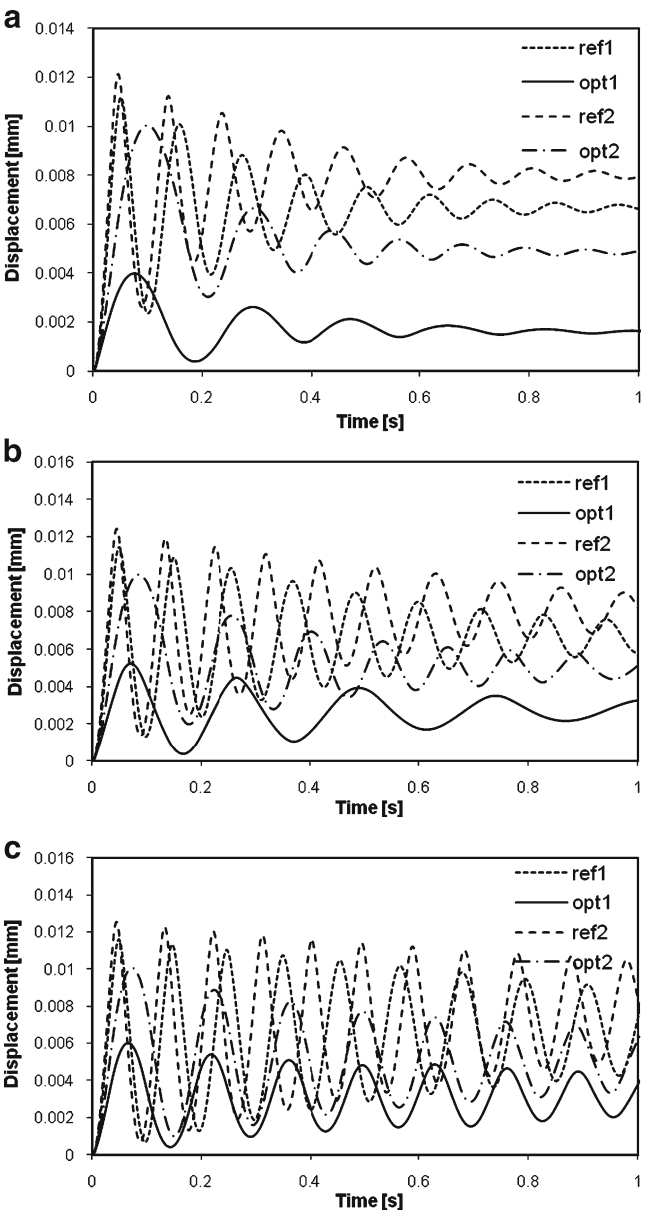

Fig. 12 Displacement of the reference (*dotted line* for $P_{0,1}$ and *dashed line* for $P_{0,2}$) and the optimized designs (*solid line* for $P_{0,1}$ and *dash-dotted line* for $P_{0,2}$): **a** $C = 400$ N.s/m, **b** $C = 200$ N.s/m, **c**) $C = 100$ N.s/m

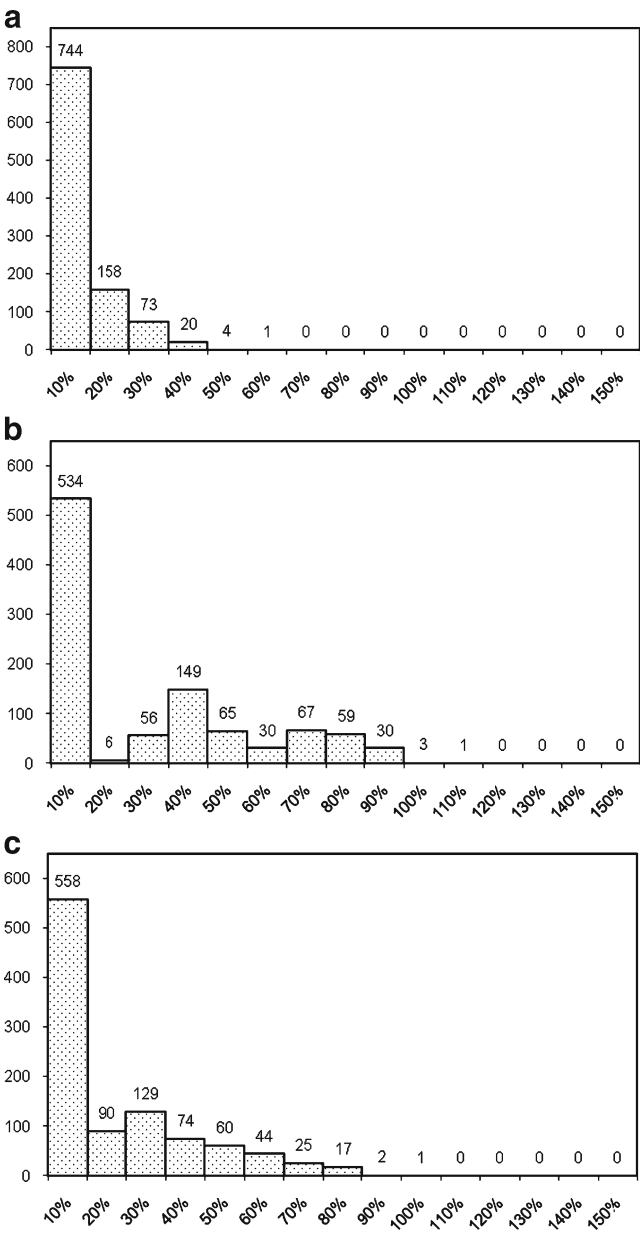

Fig. 13 Histogram of the disturbance value d defined by (10) for: **a** $C = 400$ N.s/m, **b** $C = 200$ N.s/m, **c** $C = 100$ N.s/m

$P_0 + P_1 \sin(\omega t + \varphi)$ (see Fig. 2). For the sake of simplicity it is assumed $\varphi = 0$. Numerical values were selected within the admissible intervals as $P_0 = 1{,}000$ N, $P_1 = 500$ N and $\omega = 300$ rad/s $= 47.7$ Hz. Regarding the damping coefficient, and following the previous load cases studies (see previous sections), three values were considered as $C = 400$, 200 and 100 N.s/m. Cubic Hermite interpolation was implemented in the load-displacement admissible curves, because in this case the shooting method might be necessary to obtain the steady-state response. Conversely the reference design, used for comparison, does not have continuous derivatives (see Fig. 4) and thus the respective

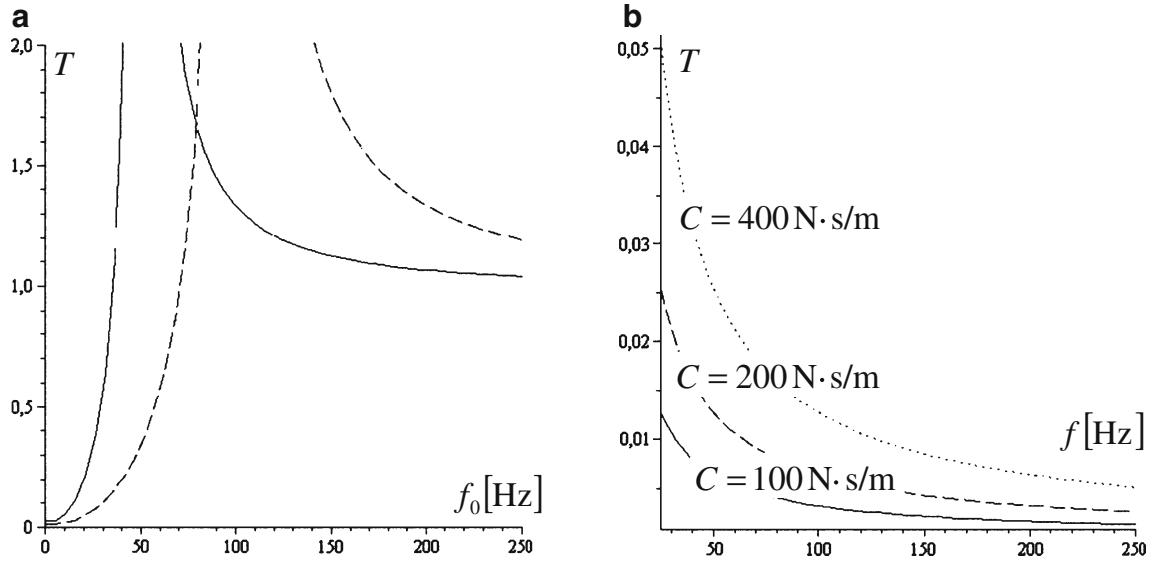

Fig. 14 **a** Transmissibility versus the natural frequency for excitation frequency $f = 50$ Hz (*solid line*) and $f = 100$ Hz (*dashed line*); **b** Transmissibility versus excitation frequency according to (15) for different values of $C = 100$ N.s/m (*full line*), 200 N.s/m (*dashed line*) and 400 N.s/m (*dotted line*), respectively

steady state solution had to be obtained by the method of long simulation.

The objective function (1) can now account for regimes, transient and steady-state one. In order to observe the effect of each of them, cases with $\gamma_{tr} = 0$, $\gamma_{st} = 1$ and $\gamma_{tr} = 0.5$, $\gamma_{st} = 0.5$ will be analyzed in this section.

In the first case, i.e. when $\gamma_{tr} = 0$ and $\gamma_{st} = 1$, the problem reduces to the minimization of transmissibility as justified in Section 2.3. Adopting dimensionless $||R|| = 1$ as stated in Section 3, one gets $O = 2P_0\,T$, where T is the transmissibility. As in Section 4.1 we will first analyze what result should be expected from the optimization. In the linear case the transmissibility T can be expressed as:

$$T = \sqrt{\frac{\omega_0^4 + \left(\frac{C}{M}\right)^2 \omega^2}{\left(\omega_0^2 - \omega^2\right)^2 + \left(\frac{C}{M}\right)^2 \omega^2}}, \tag{14}$$

where ω stands for the frequency of the excitation force and ω_0 for the natural frequency of the system. In general transmissibility is plotted with respect to the force frequency. But in our case ω is fixed and the spring rigidity (governing the natural frequency) is the design variable. Therefore the graph of transmissibility with respect to natural frequency will indicate the expected optimization result. This graph is shown in Fig. 14a) for $f = 50$ Hz and $f = 100$ Hz, corresponding to $\omega = 314$ rad/s and $\omega = 628$ rad/s.

Here it is seen that the transmissibility achieves its lowest value when the natural frequency goes to zero. Therefore the optimised load-displacement curve will tend to a curve with a plateau at the equilibrium force P_0, like for load case (1), but here the plateau will be developed only within the steady-state displacement range.

Introducing $\omega_0 = 0$ into (14), one gets:

$$T = \frac{C}{\sqrt{(M\omega)^2 + C^2}}. \tag{15}$$

Then the graph of the transmissibility versus the force frequency, for the different C values used in examples, is shown in Fig. 14b). From this graph one can see that the transmissibility values are very low and that they increase with increasing damping. Low values of transmissibility will imply a very narrow steady-state displacement range and therefore very short plateaus.

The optimised results confirmed all these predictions. In all studied cases the plateau was easily formed and the objective function achieved the analytically predicted lowest value.

Results are summarized in Table 7. The best objective function is again compared with the reference case O_{ref} and with the analytical value $O_{anl} = 2P_0T$, where T is defined by (15).

Final design load-displacement curves are shown in Fig. 15.

Table 7 Summary of the optimization analysis for the load case (iii)

C (N.s/m)	O_{fin} (N)	O_{anl} (N)	O_{ref} (N)	E (%)
400	26.66	26.66	43.86	39
200	13.34	13.33	36.07	63
100	6.67	6.67	34.95	81

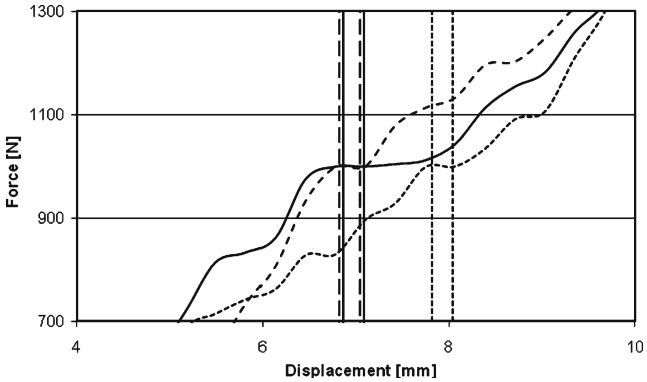

Fig. 15 Final design of the load-displacement curves (detail of the plateaus) with the range of steady-state displacements designated by *two vertical lines*, step force $P_0 = 1{,}000$ N and harmonic contribution $P_1 = 500$ N, $\omega = 300$ rad/s ($C = 400$ N.s/m *solid line*, $C = 200$ N.s/m *dashed line*, $C = 100$ N.s/m *dotted line*, $\gamma_{tr} = 0$ and $\gamma_{st} = 1$)

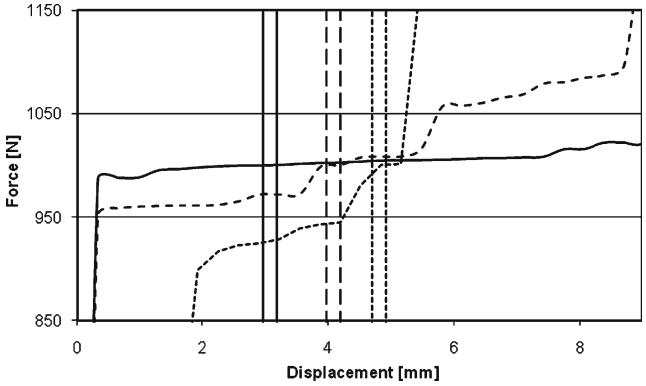

Fig. 16 Final design of the load-displacement curves (detail of the plateaus) with the range of steady-state displacements designated by *two vertical lines*, step force $P_0 = 1{,}000$ N and harmonic contribution $P_1 = 500$ N, $\omega = 300$ rad/s ($C = 400$ N.s/m *solid line*, $C = 200$ N.s/m *dashed line*, $C = 100$ N.s/m *dotted line*, $\gamma_{tr} = 0.5$ and $\gamma_{st} = 0.5$)

Objective function values are very stable in all these cases, because significant part of the load-displacement curve does not influence the total dynamic reaction in the steady-state regime. This also justifies quite a low efficiency E. Final results are very reliable and the sensitivity analysis showed that practically all disturbed designs O_{pert} are within 10% range, therefore the respective histograms are not shown.

However, all these cases show a very high reaction peak in the transient part. To neutralize this, optimization was performed assuming now contribution form both regimens i.e. $\gamma_{tr} = 0.5$ and $\gamma_{st} = 0.5$. As expected, the optimized solution is now very similar to the one obtained for load case (1). Plateau is formed at the equilibrium force level, because both regimens require it. The objective function part corresponding to the steady-state regime achieves again the analytically lowest value. Results are summarized in Table 8 and Fig. 16.

Here we note again that final results are very reliable and the sensitivity analysis showed that practically all disturbed designs O_{pert} are within 10% range, therefore the respective histograms are not shown.

Table 8 Summary of the optimization: step force $P_0 = 1{,}000$ N and harmonic contribution $P_1 = 500$ N, $\omega = 300$ rad/s, $\gamma_{tr} = 0.5$ and $\gamma_{st} = 0.5$

C (N.s/m)		O_{fin} (N)	O_{ref} (N)	E (%)
400	O	45.4	1,167	96
	$\gamma_{tr} A_{tr}$	32.1	1,145	97
	$\gamma_{st} A_{st}$	13.3	22	39
200	O	83.8	1,350	94
	$\gamma_{tr} A_{tr}$	77.1	1,332	89
	$\gamma_{st} A_{st}$	6.7	18	63
100	O	282.0	1,471	81
	$\gamma_{tr} A_{tr}$	278.6	1,453	62
	$\gamma_{st} A_{st}$	3.4	17	80

4.4 Load case (iv)—set of step loads with harmonic components

This load case corresponds to the situation where the structure is designed to withstand several step loads with harmonic components, not simultaneously applied.

Four step forces with superimposed a harmonic component are considered: namely the step loads $P_{0,1} = 600$ N, $P_{0,2} = 800$ N, $P_{0,3} = 1{,}000$ N, $P_{0,4} = 1{,}200$ N and the respective harmonic forces $P_{1,1} = 600$ N, $P_{1,2} = 500$ N, $P_{1,3} = 400$ N, $P_{1,4} = 300$ N. The respective harmonic component frequency are, $\omega_1 = 191.0$ Hz, $\omega_2 = 143.2$ Hz,

Table 9 Summary of the optimization results of the load case (iv)

C (N.s/m)	Step	O_{fin} (N)	O_{anl} (N)	O_{ref} (N)	E (%)
400	O	10.89	10.89	14.3	23.8
	$\lambda_1 O_1$	2.00	2.00	2.11	5.0
	$\lambda_2 O_2$	2.22	2.22	2.44	9.1
	$\lambda_3 O_3$	2.67	2.67	3.18	16.1
	$\lambda_4 O_4$	4.00	4.00	6.58	39.2
200	O	5.45	5.44	10.25	46.8
	$\lambda_1 O_1$	1.00	1.00	1.19	16.1
	$\lambda_2 O_2$	1.11	1.11	1.48	24.9
	$\lambda_3 O_3$	1.34	1.33	2.17	38.4
	$\lambda_4 O_4$	2.00	2.00	5.41	63.0
100	O	2.72	2.72	8.90	69.7
	$\lambda_1 O_1$	0.50	0.50	0.81	38.0
	$\lambda_2 O_2$	0.56	0.56	1.09	49.1
	$\lambda_3 O_3$	0.67	0.67	1.86	64.1
	$\lambda_4 O_4$	1.00	1.00	5.24	80.9

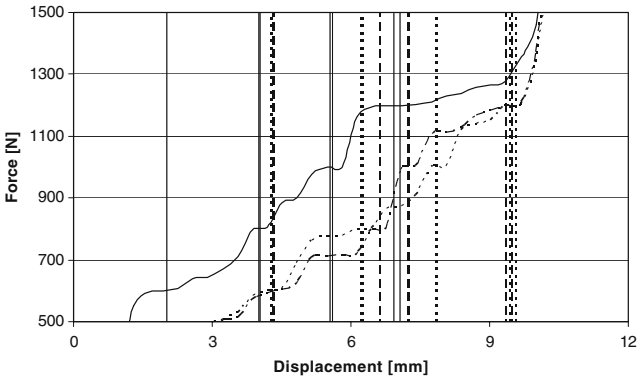

Fig. 17 Final design of the load-displacement curves (detail of the plateaus) with the range of steady-state displacements designated by *two vertical lines*, load case (4) (C = 400 N.s/m *solid line*, C = 200 N.s/m *dashed line*, C= 100 N.s/m *dotted line*, $\gamma_{tr} = 0$ and $\gamma_{st} = 1$)

$\omega_3 = 95.5$ Hz and $\omega_4 = 47.7$ Hz. The phase angle is zero in all cases. Probability of occurrence is assumed equal, $\lambda_1 = \lambda_2 = \lambda_3 = \lambda_4 = 0.25$. The cost function O is then defined according to (4) adding the contribution of each partial value O_i, i = 1, ..., 4. In this example only the steady state contribution is considered, so we set $\gamma_{tr} = 0$ and $\gamma_{st} = 1$. Results are summarized in Table 9.

It is interesting here to note the fairly even contribution of each individual force (see the different $\lambda_i O_i$ values) and the agreement between the analytical solution O_{anl} and the final ("optimal") one O_{fin}.

Optimized load-displacement curves are shown in Fig. 17. It can be concluded that plateau formation at the respective forces levels is easily realized because the respective steady-state displacement range is very small and thus the plateaus do not obstruct each other. Final design is also very reliable and the sensitivity analysis showed that practically all disturbed designs O_{pert} are within a 10% range.

5 Conclusions

The model described in this work, even though one dimensional, captures well the mechanical problem and the main issues that should be tackled in passive vibration control. Due to the diversity of loads that this type of systems are subjected the optimization criterion implemented is quite general. Depending on the situation it may include transient and steady state contributions and different loads not simultaneously applied.

From the results obtained it is apparent that optimal behaviour can be achieved, however it is also evident that the optimal solution is highly dependent on the problem data, namely applied forces and constraints. Thus a precise definition of existing forces and design constraints is crucial for its success in practical applications. Evidently, optimal design obtained for a particular loading set-up may not be efficient for another one. Nevertheless, the computational tool is quite efficient, depending on the example results were obtained within 10 min to 3 h on a 2 GB RAM portable Intel Core Duo T7500 PC, therefore it is worthwhile to use it for obtaining general ideas and guidelines about the non-linear load-displacement curve optimal shape.

Once the optimal load-displacement curve(s) is identified future research will be directed to the design of cellular and/or composite viscoelastic materials achieving this behaviour(s). This application will have a direct and immediate impact on product design and development, especially in the design of new mechanical components such as engine mounts and /or suspension systems.

Acknowledgement Support from Grant PTDC/EME-PME/67658/2006: "Design of cellular elastomeric materials for passive vibration control" FCT-PORTUGAL, is gratefully acknowledged.

Appendix A

An efficient numerical iterative method, which can be used to determine the steady-state part of the system response, is presented. The method is known as the Shooting Method (see Jirásek 1988) where it is presented for nonlinear undamped second order equation). It also performs well in dynamically unstable systems, where several periodic solutions may exist. When the dynamic response is chaotic, the method diverges.

The Shooting Method requires rewriting (7) as a system:

$$\dot{x}_1(t) = x_2(t)$$
$$\dot{x}_2(t) = \left(-F(x_1(t)) - Cx_2(t) + P(t)\right)/M, \tag{16}$$

with $x_1(t) = u(t)$ and $x_2(t) = \dot{u}(t)$.

Let the period of the steady-state regime be T. In compact form the system (16) can be written as:

$$\dot{\mathbf{x}}(t) = \mathbf{f}(\mathbf{x}(t), t) \tag{17}$$

with the initial condition $\dot{\mathbf{x}}(0) = \mathbf{x}_0$.

The shooting function $\mathbf{h}$ is defined as a mapping, which attributes to each initial state $\mathbf{x}_0$ the system state at the time, which corresponds to the known period T:

$$\mathbf{h} : \Re^2 \rightarrow \Re^2$$
$$\mathbf{h}(\mathbf{x}_0) = \mathbf{x}_T. \tag{18}$$

The objective is to find the fixed point of the shooting function, $\mathbf{h}(\mathbf{x}_F) = \mathbf{x}_F$, i.e. to find the initial conditions $\mathbf{x}_F$ ensuring that the solution is periodic with the period T.

If $\mathbf{x}_0$ is an initial choice of initial conditions, then the solution $\mathbf{x}_F$ can be found by an iterative procedure based on the Newton–Raphson method as:

$$\mathbf{x}_{n+1} = \mathbf{x}_n + \left(\mathbf{I} - \frac{\partial \mathbf{h}}{\partial \mathbf{x}}(\mathbf{x}_n)\right)^{-1} \cdot (\mathbf{h}(\mathbf{x}_n) - \mathbf{x}_n), \tag{19}$$

where $n = 0, 1, 2, \ldots$ and $\mathbf{I}$ is the 2×2 unit matrix.

The crucial point in this process is to obtain for each iteration $(\mathbf{x}_n)$ the Jacobian matrix of the shooting function

$$h_{i,j}(\mathbf{x}_n) = \frac{\partial h_i}{\partial x_j}(\mathbf{x}_n) \quad i, j = 1, 2. \tag{20}$$

In Jirásek (1988) it is proven that these derivatives correspond to the solution of the linearized homogeneous system, expressed at the value of the solution of the current iteration, with the initial conditions in the form of the base vectors. To justify this, let the initial conditions be chosen as $\mathbf{x}(0) = \mathbf{p}$. Then the solution of the system (16) with these initial conditions can be designated as $\mathbf{r}(\mathbf{p}, t)$. Therefore from (17):

$$\begin{aligned} &\mathbf{r}(\mathbf{p}, 0) = \mathbf{p}, \quad \forall \mathbf{p} \in \Re^2 \\ &\frac{\partial \mathbf{r}}{\partial t}(\mathbf{p}, t) = \mathbf{f}(\mathbf{r}(\mathbf{p}, t), t), \quad \forall \mathbf{p} \in \Re^2, \forall t \in \Re_0^+ \end{aligned} \tag{21}$$

Integrating (21) one obtains:

$$\mathbf{r}(\mathbf{p}, t) = \mathbf{p} + \int_0^t \mathbf{f}(\mathbf{r}(\mathbf{p}, \tau), \tau)\, d\tau, \quad \forall \mathbf{p} \in \Re^2, \forall t \in \Re_0^+. \tag{22}$$

Now the shooting function can be written as:

$$\mathbf{h}(\mathbf{p}) = \mathbf{r}(\mathbf{p}, T). \tag{23}$$

Thus,

$$\mathbf{h}(\mathbf{p}) = \mathbf{p} + \int_0^T \mathbf{f}(\mathbf{r}(\mathbf{p}, \tau), \tau)\, d\tau \tag{24}$$

and now the Jacobian matrix can be calculated. Derivative evaluation at the fixed boundary conditions $\mathbf{p} = \mathbf{x}_0$, gives,

$$\begin{aligned} \frac{\partial \mathbf{h}}{\partial \mathbf{p}}(\mathbf{x}_0) &= \frac{\partial \mathbf{r}}{\partial \mathbf{p}}(\mathbf{x}_0, T) \\ &= \mathbf{I} + \int_0^T \frac{\partial \mathbf{f}}{\partial \mathbf{x}}(\mathbf{r}(\mathbf{x}_0, \tau), \tau)\, \frac{\partial \mathbf{r}}{\partial \mathbf{p}}(\mathbf{x}_0, \tau)\, d\tau \end{aligned} \tag{25}$$

Thus we can define the Jacobian matrix function $\mathbf{H}(t)$,

$$\mathbf{H}(t) = \mathbf{I} + \int_0^t \frac{\partial \mathbf{f}}{\partial \mathbf{r}}(\mathbf{r}(\mathbf{x}_0, \tau), \tau)\, \frac{\partial \mathbf{r}}{\partial \mathbf{p}}(\mathbf{x}_0, \tau)\, d\tau, \tag{26}$$

and by differentiation one gets,

$$\begin{aligned} &\dot{\mathbf{H}}(t) = \frac{\partial \mathbf{f}}{\partial \mathbf{x}}(\mathbf{r}(\mathbf{x}_0, t), t)\, \mathbf{H}(t), \\ &\mathbf{H}(0) = \mathbf{I}. \end{aligned} \tag{27}$$

From (27) we conclude that the shooting function Jacobian matrix, for each iteration, corresponds to the solution of a new linearized system, in which the coefficients are obtained from the original system by differentiation and substitution of the previous solution.

We have tested the methodology also in the case of the standard material model. Then the system must be written in the form:

$$\begin{aligned} \dot{x}_1(t) &= x_2(t), \\ \dot{x}_2(t) &= (-F_1(x_1(t)) - F_2(x_3(t)) + P(t))/M, \\ \dot{x}_3(t) &= x_2(t) - F_2(x_3(t))/C, \end{aligned} \tag{28}$$

where $x_1(t) = u_1(t)$, $x_2(t) = \dot{u}_1(t)$, $x_3(t) = u_2(t)$.

It is also possible to extend the methodology to the complex domain, where the Jacobian matrix has dimensions 4×4, because it is necessary to deal separately with the real and the imaginary parts of the displacement and velocity.

Here it is important to mention that derivative continuity requires the spline Hermite interpolation to approximate load-displacement curve.

References

Balandin DV, Bolotnik NN, Pilkey WD (2001) Optimal protection from impact, shock and vibration. Gordon and Breach Science Publishers, New York

Fritsch FN, Carlson RE (1980) Monotone piecewise cubic interpolation. SIAM J Numer Anal 17(2):238–246

Jirásek M (1988) Simple non-linear system simulation. Internal Report, Czech Technical University in Prague (in Czech)

Jones DIG (2001) Handbook of viscoelastic vibration damping. Wiley, New York

Kirkpatrick S, Gelatt CD Jr, Vecchi MP (1983) Optimization by simulated annealing. Science 220(4598):671–680

Kovacic I, Brennan MJ, Waters TP (2008) A study of a nonlinear vibration isolator with a quasi-zero stiffness characteristics. J Sound Vib 315:700–711

Lakes RS (2001) Extreme damping in composite materials with a negative stiffness phase. Phys Rev Lett 86(13):2897–2900

Lakes RS (2002) High damping composite materials: effect of structural hierarchy. J Compos Mater 36(3):287–297

Meirovitch L (1975) Elements of vibration analysis. McGraw-Hill Kogakusha, Tokyo

Platus DL (1993) Smoothing out bad vibes. Mach Des 26:123–130
Prasad J, Diaz AR (2008) A concept for a material that softens with frequency. J Mech Des 130(9):091703.1–091703.7
Pritz T (1998) Frequency dependences of complex moduli and complex Poisson's ratio of real solid materials. J Sound Vib 214(1):83–104
The MathWorks, Inc. (2007) Release R2007a documentation for MATLAB. The MathWorks, Inc., Massachusetts
Zavala PG, Pinto MG, Pavanello R, Vaqueiro J (2000) Experimental and computational simulation approaches for engine mounting development and certification. SAE technical paper series 2000-01-3239E